Heliyon 10 (2024) e35372

Contents lists available at ScienceDirect

Heliyon

journal homepage: www.cell.com/heliyon

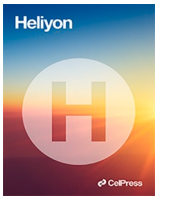

Research article

Characterization of MSCs expressing islet neogenesis associated protein (INGAP): INGAP secretion and cell survival *in vitro* and *in vivo*

Maria Petropavlovskaia [a,b,1,*], Beatrice Assouline-Thomas [a,1], Jessica Cuerquis [a,1], Jing Zhao [a], Shaun Violette-Deslauriers [a,b], Eni Nano [a,b], Nicoletta Eliopoulos [a,b], Lawrence Rosenberg [a,b]

[a] *Lady Davis Institute for Medical Research, SMBD-Jewish General Hospital, Montreal, QC, Canada*
[b] *Department of Surgery, Faculty of Medicine and Health Sciences, McGill University, Montreal, QC, Canada*

A R T I C L E I N F O

Keywords:
Mesenchymal stem cells (MSCs)
Mesenchymal stromal cells
Islet neogenesis associated protein (INGAP)
Extracellular matrix
Adipogenic differentiation
Hydrogel

A B S T R A C T

Mesenchymal stem/stromal cells (MSCs) are emerging as a new therapy for diabetes. Here we investigate the properties of MSCs engineered to express Islet Neogenesis Associated Protein (INGAP) previously shown to reverse diabetes in animal models and evaluate their potential for anti-diabetic applications in mice. Mouse bone marrow-derived MSCs retrovirally transduced to co-express INGAP, Firefly Luciferase and EGFP (INGAP-MSCs), were characterized *in vitro* and implanted intraperitoneally (IP) into non-diabetic and diabetic C57BL/6 mice (Streptozotocin model) and tracked by live bioluminescence imaging (BLI). Distribution and survival of IP injected INGAP-MSCs differed between diabetic and non-diabetic mice, with a rapid clearance of cells in the latter, and a stronger retention (up to 4 weeks) in diabetic mice concurring with homing towards the pancreas. Interestingly, INGAP-MSCs inhibited the progression of hyperglycemia starting at day 3 and lasting for the entire 6 weeks of the study. Pursuing greater retention, we investigated the survival of INGAP-MSCs in hydrogel matrices. When mixed with Matrigel™ and injected subcutaneously into non-diabetic mice, INGAP-MSCs remained in the implant up to 16 weeks. *In vitro* tests in three matrices (Matrigel™, Type I Collagen and Vitro-Gel®-MSC) demonstrated that INGAP-MSCs survive and secrete INGAP, with best results at the density of 1–2 x 10^6 cells/mL. However, all matrices induced spontaneous adipogenic differentiation of INGAP-MSCs *in vitro* and *in vivo*, which requires further investigation of its potential impact on MSC therapeutic properties. In summary, based on their ability to stop the rise in hyperglycemia in STZ-treated mice, INGAP-MSCs are a promising therapeutic tool against diabetes but require further research to improve cell delivery and survival.

* Corresponding author. Lady Davis Institute for Medical Research, SMBD-Jewish General Hospital, Department of Surgery, Faculty of Medicine, McGill University, 3755 Cote Ste-Catherine Rd, Montreal, QC, H3T 1E2, Canada.
E-mail address: maria.petropavlovskaya@mcgill.ca (M. Petropavlovskaia).
[1] Maria Petropavlovskaia, Beatrice Assouline-Thomas and Jessica Cuerquis contributed equally to this work.

https://doi.org/10.1016/j.heliyon.2024.e35372
Received 21 November 2023; Received in revised form 25 July 2024; Accepted 26 July 2024
Available online 31 July 2024

1. Introduction

Diabetes Mellitus (DM) is caused by a significant loss of insulin-producing beta cells in the pancreas. In Type 1 DM (T1DM), beta cell death is driven by autoimmunity, while in Type 2 (T2DM), insulin resistance, oxidative stress and inflammation are implicated as main causes [1]. Despite significant reduction, even in the long-standing cases of T1D, the pancreas contains residual functional beta cells, estimated to range from ~2 to 40 % of the original beta cell mass [2], with some evidence of islet neogenesis [3]. This raises hope that the restoration of beta cell mass through preservation of existing beta cells and through endogenous regeneration is possible and inspires the development of combinatorial strategies involving the regenerative, anti-inflammatory and immunomodulatory therapies. The goal of this study was to develop such a strategy using Mesenchymal Stromal/Stem Cells (MSCs), known for their anti-inflammatory and immunomodulatory properties, engineered to express and secrete a regenerating factor, Islet Neogenesis Associated Protein (INGAP).

MSCs have generated a lot of interest as a potential therapy for diabetes not only due to the reported instances of induced differentiation into insulin-producing cells [4], but mostly because of their anti-inflammatory, anti-apoptotic, angiogenic, mitogenic and immunomodulatory properties [5]. Importantly, MSCs have been shown to promote the survival of pancreatic islets and decrease inflammation [6,7]. Clinical efficacy and safety of MSCs for T1DM and T2DM treatment has been evaluated in over 80 clinical trials using MSCs derived from different sources (www.clinicaltrials.gov), resulting in several meta-analyses that show an overall improvement in C-peptide values after 6–12 months of treatment with MSCs [8–10]. Importantly, MSCs derived from T1DM patients are also suitable for this therapeutic approach, exhibiting potency comparable to healthy controls (including immunomodulatory) *in vitro* [11,12], and in T1DM patients [13,14]. These encouraging data provide the rationale for further research on MSCs as a safe and promising strategy to intervene in disease progression and preserve beta cell function [13].

The therapeutic potential of MSCs can be further enhanced by gene therapy [15]. For instance, MSCs overexpressing VEGF and IL-1 receptor antagonist have been shown to improve islet survival and the outcome of islet transplantation [16]. We hypothesized that MSCs expressing beta cell specific regenerating factor(s) may stimulate endogenous regeneration and improve beta cell survival. INGAP, the first therapeutic candidate with islet neogenic activity, was discovered in our earlier studies as a secreted, 16.8 kDa protein stimulating formation of new islets in the duct-obstructed hamster pancreas [17]. It belongs to the Reg-3 family of regenerating proteins found in many species, including humans. However, no human analog of INGAP has been identified either by sequence homology (INGAP is Reg3δ, found only in hamsters and mice [18]) or by the ability to induce islet neogenesis [19]. INGAP activity appears to be mediated through its bio-active peptide, $INGAP^{104\text{-}118}$ [17,20], shown to stimulate islet neogenesis and reverse diabetes in animal models [19,21], improve islet survival and function [22], induce proliferation of beta cells [23] and endocrine differentiation of human ductal cells [24,25]. In clinical trials (Phase 2), $INGAP^{104\text{-}118}$ increased C-peptide in T1DM patients and improved glycaemic control in T2DM patients after 90 days of daily injections, which was very promising [26]. However, further clinical use of $INGAP^{104\text{-}118}$ was limited due to its short half-life and the need for frequent injections. To achieve optimal clinical response, a longer-term exposure, controlled release, better formulations or combination with other therapies (immunomodulatory for T1DM) were suggested [26]. A gene therapy approach for INGAP delivery may solve these issues by establishing a continuing expression of INGAP in the body, while combination with MSCs may further help to achieve both regenerative and immunomodulatory and anti-inflammatory effects. This provided the rationale for generating INGAP-expressing MSCs and evaluating the potential of this novel approach for the treatment of diabetes.

Here, we describe the generation of INGAP-MSCs (mouse bone marrow-derived) using the full-length INGAP protein encoded in a retroviral vector AP2 [27], along with Luciferase and EGFP, and characterize their potential for cell therapy in normal and STZ-treated mice focusing on cell survival and distribution.

2. Materials and Methods

2.1. Cell culture

Mouse bone-marrow MSCs were derived from tibias and femurs of C57BL/6 mice as described [28] and cultured in 150 mm tissue culture plates (Sarstedt, Montreal, Quebec, Canada) in α-MEM medium (Gibco™ Life Technologies, Ontario, Canada) supplemented with 10 % FBS, v/v, (Wisent, Quebec, Canada), L-glutamine 200 mM and penicillin-streptomycin 100 U/mL (Gibco™), under normoxia. Cells were expanded by passaging at 80–90 % confluency (seeding density 1-2 x 10^3 cells/cm^2) and were frozen (10^6 cells/mL in α-MEM medium with 10 % DMSO and 50 % FBS) at passage 16 and less for future use. Cells were counted using hemocytometer and the doubling time was calculated using the equation $Td = t \times Ln(2)/Ln(Nt/No)$, where "t" is time in culture and N is cell number at inoculation (No) and at t hour of culture (Nt).

CHO–K1 and rat insulinoma RINm5F cells were purchased form ATCC and cultured in 10 cm tissue culture plates (Sarstedt) in RPMI-1640 (Gibco™) supplemented with 10 % FBS and penicillin-streptomycin 100 U/mL under normoxia and passaged every 3–4 days.

2.2. Generation of retroviral construct for INGAP expression

1). **Addition of the C-terminal tag (FLAG®** (Sigma) also known as **DYKDDDDK** or **DDK** tag (used here): INGAP cDNA subcloned in the pcDNA™ 3.1/V5-His TOPO™ vector (Invitrogen, Thermo-Fisher), was excised with *Hin*dIII and *Eco*RV and ligated into pCMV6-Entry vector (OriGene, Rockville, MD) encoding the DDK tag, as shown in Supplementary Fig. 1A. The resulting INGAP-DDK/pCMV6

plasmid was amplified in *E. coli* bacteria (DH5α, Thermo-Fisher), purified using mini- and maxi prep kits (Qiagen), and sequenced (Genome Quebec Innovation Centre, Montreal, QC).

Transient transfection of CHO–K1 cells (OPTI-MEM medium (Gibco™) and Lipofectamine 3000 (Thermo-Fisher)) was used to verify the tag expression with anti-FLAG/DDK antibody (Santa-Cruz) (Supplementary Fig. 1B). Size of 18.9 kDa of secreted INGAP-DDK were confirmed by Western blotting of conditioned medium (CM) using the custom-made polyclonal anti-INGAP antibody to the N-terminal peptide (GenScript) that also reacts with rINGAP [20] (Supplementary Fig. 2A). Prior to generating a retroviral construct described below, biological activity of INGAP-DDK (hereinafter INGAP) was verified using RINm5F cells, as established in previous publications [23,29] and described in detail in Supplementary Figs. 2B–D.

In addition, RINm5F cells were stably transfected with INGAP-DDK/pCMV6 (selection with Geneticin™ (G418 sulfate) at 1 mg/mL; Gibco™, Invitrogen). CM from the resulting clone R4 (R4-CM), collected after 48h in serum-free RPMI and containing ~ 0.5 μM INGAP was used for preparing standard curves for INGAP quantification.

2). **PCR cloning of tricistronic construct using retroviral plasmid AP2** (MSCV promoter and IRES-EGFP) [27] (Supplementary

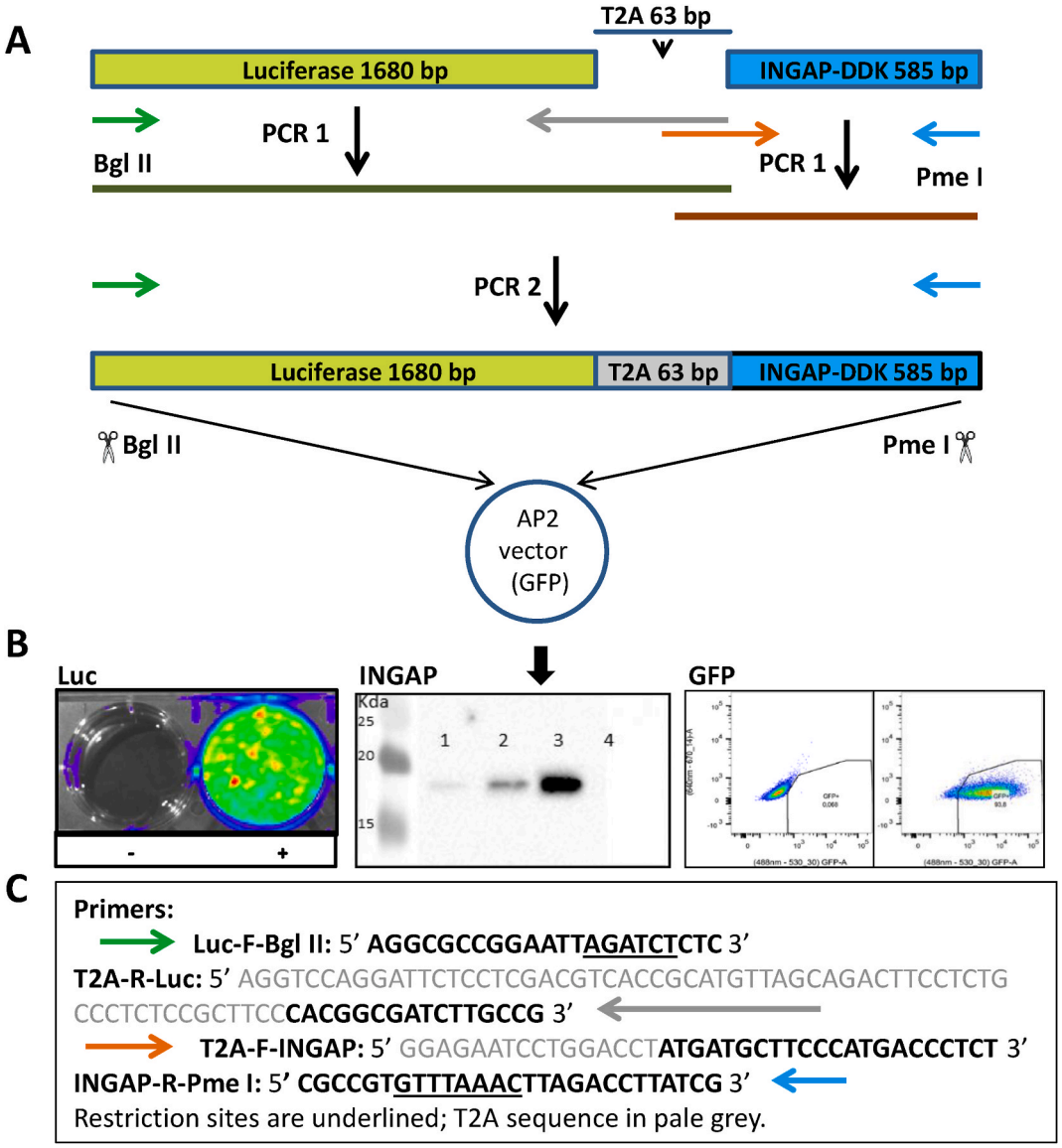

Fig. 1. Generation of MSCs expressing Luc-INGAP-GFP construct encoded in a tricistronic AP2 vector.
A. PCR cloning scheme to generate a retroviral vector AP2 encoding Luc-T2A-INGAP construct (primer sequences are shown in (**C**)); **B**. Resulting INGAP-MSCs express Luc, INGAP and GFP: Luc activity was detected by IVIS Spectrum in Luciferin–treated cells – Wild-type (WT)-MSCs (−) and INGAP-MSCs (+); INGAP secretion was detected by Western blot analysis of CM from INGAP-MSCs (Lanes 1–3, 2x increasing volumes) and WT-MSC (lane 4, same volume as lane 2). Blots were probed with anti-INGAP antibody); GFP expression analyzed by FACS (93.8 % of the cells are GFP+). **C.** Primers used for PCR cloning.

Fig. 3): to co-express EGFP with INGAP and Firefly Luciferase (Luc), Luc sequence from the MIG-Luciferase-IRES-GFP plasmid (Addgene, #75021, created and provided by Saradhi Mallampati, The University of Texas M.D. Anderson Cancer Center), was used. *Bgl*II restriction site positioned upstream of the ORF was included in the forward primer Luc-F-*Bgl*II (sequences are shown in Fig. 1C). To co-express Luc and INGAP from a single mRNA, the T2A peptide was inserted by overlap extension PCR, using T2A sequences (both sense and antisense) as overhangs in the PCR primers for INGAP and Luc. Q5® High-Fidelity DNA Polymerase (New England Biolabs) was used for all reactions. Extended PCR 1 products for INGAP and Luciferase were gel-purified (QIAquick Gel Extraction kit, Qiagen) and spliced into a single PCR product using the "end" primers for Luciferase and INGAP. Upon purification, the Luciferase-T2A-INGAP PCR product was digested with *Bgl*II and *Pme*I and ligated into similarly restricted AP2 plasmid, upstream of IRES-GFP. The resulting construct, Luc–T2A-INGAP–IRES-GFP named AP2-INGAP was amplified in DH5α *E.coli* cells, purified and sequenced, as above.

An "empty vector" control plasmid, Luc-T2A′–IRES-GFP (named AP2-Luc), was created by PCR using AP2-INGAP as a template. Luc-F-*Bgl*II forward primer and the reverse primer including the *Pme*I restriction site (underlined), 5′ GTCCGTGTTTAAAC**TTA**TCCAGGATTCTCC 3′ and the stop codon replacing the last Proline in T2A peptide (in bold) were used. Restriction digest and ligation were done as above.

2.3. Production of retroviral particles and transduction of mouse MSCs

Recombinant retroparticles were produced by the established protocol in GP2-293 packaging cells using Lipofectamine 3000, as described previously [30]. First batch of virus-containing medium was collected 24 h post-transfection, stored at 4 °C and pooled with the second batch (52 h post-transfection), spun, filtered with 0.45 μm filter, and concentrated 60x with Lenti-X Concentrator (Clontech/Takara) for immediate use or stored at −80 °C.

MSCs plated at 1×10^5 cells/well in 6-well plates were exposed to 10 μL concentrated viral medium for 48 h, followed by medium change and 24 h cell recovery, and transduced again (total 4 times). Post transduction, cells were expanded and sorted by FACS for EGFP (BD LSR Fortessa™, flow cytometer (Becton Dickinson) at the LDI Flow Cytometry Core Facility followed by freezing and storage in liquid nitrogen. Expression of INGAP-DDK was confirmed by Western blot analysis of MSC-INGAP CM, using anti-INGAP (custom-made by Genscript to the N-terminal peptide) and anti-DDK (Thermo-Fisher or Genscript) antibodies. Expression and activity of Luciferase was verified by adding D-Luciferin (150 μg/mL) to the cells and imaging by IVIS® Spectrum CT (PerkinElmer). Also, expression of all target proteins was confirmed by immunostaining (Supplementary Fig. 4).

Production of recombinant INGAP (rINGAP) and preparation of standards for quantification: As previously described [20], rINGAP (17.6 kDa, 6His-tagged) was produced in the suspension cultures of stably transduced 293-SF cells and purified from CM by Cobalt affinity resin (Takara Bio) followed by HPLC purification (IRIC, University of Montreal). Concentration of rINGAP reconstituted in PBS was determined by OD280 and adjusted to 1 μM for further experiments. For quantification of INGAP secretion in the INGAP-MSC CM, 2-fold serial dilutions of purified rINGAP or R4-CM (in serum-free RPMI), ranging from 0.5 to 8 pmol/μL, were prepared.

2.4. Analysis of INGAP secretion in INGAP-CHO and INGAP-MSC conditioned media (CM)

To estimate INGAP secretion rate, we used Western blot densitometry to determine INGAP concentration in CM, using the known quantities of HPLC-purified rINGAP protein for standards. We took advantage of the ChemiDoc™ MP system with a dynamic range greater than four orders of magnitude allowing for an accurate densitometry of protein bands. For collection of CMfrom INGAP-MSCs, culture medium containing 10 % FBSwas replaced for 24–48h with serum-free OPTI- MEM medium (Gibco™) found to support MSC growth and be compatible with SDS-PAGE.

CM from transiently transfected CHO–K1 (INGAP-CHO, 5–20 μL) and from INGAP-MSCs (20 and 40 μL) were resolved on a 12.5 % SDS-PAGE, transferred to a Nitrocellulose membrane (BioRad, Mississauga, Canada) and probed with the primary (anti-INGAP, rabbit) and secondary (HRP-conjugated anti-rabbit) antibodies. Chemiluminescent detection of HRP and quantification was done using Clarity Western ECL Substrate, ChemiDoc™ MP and ImageLab software (BioRad). A blank sample and four rINGAP or R4-CM standards (2-fold dilution series) were run on the same gel. To ensure the accuracy of quantification, densitometry for all samples was performed before the signal saturation point. The derived standard curve (acceptable at $R^2 > 0.990$) was used to determine INGAP amounts in the CM samples. An example of such quantification is shown in Supplementary Fig. 5.

2.5. MSC differentiation assay

Cell differentiation assay was carried out as previously [30]. Briefly, wild type (WT) MSCs and INGAP-MSCs grown in 6-well plates, were exposed to the differentiation media, as before [30], changed twice a week, or the regular growth medium (negative control). Duration of the adipogenic differentiation was one week, while the osteogenic differentiation lasted 4.5 weeks.

Following fixation with paraformaldehyde (4 % in PBS, v/v), differentiation was verified by Oil Red O staining (adipogenic) or by 1 % Alizarin Red S, w/v, (Sigma) (osteogenic) [30]. Cells were photographed using a Leica DMIL microscope.

Chondrogenic differentiation was assessed in INGAP-MSCs using StemXVivo Human/Mouse Chondrogenic kit (R&D Systems). Cells (1.25×10^5) were cultured in 15 mL tubes as biomass pellets for 21 days, fixed in 10 % buffered formalin and stained with Alcian Blue (1 % in 0.1 N HCl, w/v, Sigma) for 1h. Pellets were photographed using Leica MZ10F microscope, embedded in paraffin, sectioned (5 μm) and imaged using Axioscan 7 system (Zeiss). Nuclei were counterstained with Neutral Red.

2.6. Immunophenotypic characterization of MSCs by flow cytometry

MSCs were trypsinized, washed with cold 2 % FBS + DPBS, v/v (staining buffer), spun at 1200 rpm (350g) for 5 min at 4 °C, counted, resuspended in cold staining buffer at 1×10^7 cells/mL and kept on ice for 30 min. 30 μL aliquots (3×10^5 cells) were distributed to 1.5 mL tubes and incubated with antibodies (Supplementary Table 1) for 30 min on ice, in the dark, washed twice with cold staining buffer and transferred to FACS tubes for processing on BD LSRFortessa™ flow cytometer (Becton Dickinson). The gating strategy is illustrated in Supplementary Fig. 6. The data were analyzed with the FlowJo software.

2.7. Implantation of INGAP-MSCs in C57BL/6 mice

All animal work was performed at the LDI Animal Care Facility, in accordance with the Guidelines of the Canadian Council on Animal Care. Animal protocols were approved by the Animal Care Committee of McGill University. C57BL/6 mice, male, 6–8 weeks of age were purchased from Charles River Laboratories and kept under standard conditions and chow.

Induction of diabetes was carried out by a single injection of Streptozotocin (Sigma-Aldrich, 125 mg/kg of body weight) prepared in sodium citrate buffer (pH 4.5) administered following a 6 h fast. Glycemia (non-fasting) was tested at day 3 and 7 from the tail-tip blood sample using Contour Next (Ascensia Diabetes Care) glucometer. Mice with glycemia >13 mM twice by day 7 were considered diabetic and randomized into groups of 8 mice with glycemia in the range 13–25 mM. During treatments, body weight and non-fasting glycemia were measured weekly for 6 weeks.

Cell preparation: INGAP-MSCs were trypsinized, washed with RPMI-1640 medium (serum-free and not supplemented with antibiotics, etc.) and counted. Each diabetic mouse (n = 8) received 10^7 cells in 450 μL of RPMI via intraperitoneal (IP) injection or an equivalent volume of RPMI. Non-diabetic mice (n = 8) were injected IP with 5×10^6 cells/450 μL of RPMI per animal and followed by live bioluminescence (BLI) weekly. For Matrigel-based implantation, 5×10^6 cells in 150 μL of RPMI were mixed with 400 μL Matrigel on ice and immediately injected subcutaneously, on the back of the anesthetized mouse. 24 h prior to BLI, mice were depilated with Nair solution, under isoflurane anesthesia.

***In vivo* bioluminescence (BLI) imaging** was done weekly using IVIS® Spectrum CT imager (Min. Detectable Radiance: 70 photons/s/sr/cm2) after IP injection of Luciferin (PerkinElmer, 150 mg/kg of body weight in 200 μL of PBS, 100 μL on each side). A kinetic curve was performed during the first assay to determine the timing of the peak of bioluminescence, used thereafter for all imaging sessions. Mice were imaged in groups of 4 and always in the same order to minimize variability in BLI detection. Although BLI cannot be used for accurate quantification of cell numbers, the signal intensity correlates with the cell presence and presents a useful estimate of the cellular dynamics in the tissue.

Upon euthanasia, Matrigel implants and pancreata were removed and fixed in 10 % formalin. Processsing, sectioning and Immunohistochemistry for Insulin were performed at the Segal Cancer Centre Research Pathology Facility (RPF) of the JGH using standard techniques. Pancreatic sections (4 μm) spaced with at least 150 μm interval were incubated with rabbit polyclonal anti-insulin antibody (1:100, Santa Cruz Biotechnology), followed by the OmniMap anti-Rabbit-HRP and ChromoMap-DAB kits, counterstained with Hematoxylin and imaged using the Aperio AT Turbo Scanner (Leica Biosystems). Implant sections were stained with Hematoxylin-Eosin followed by imaging as above or probed with anti-INGAP rabbit antibody (1:100)/anti-rabbit Alexa-Fluor-488 2nd antibody (1:500, Jackson Laboratories) and mounted with Vectashield HardSet medium (with DAPI, Vector Laboratories) for imaging by FV10i confocal microscope (Olympus).

Morphometric analysis of the pancreatic sections (3 per each pancreas) was assisted by Fiji/ImageJ [31] and ImageScope (Leica Biosystems) software and included counting islets (containing ≥5 cells), measurements of the islet area in μm^2 and counting beta cells in each islet. Beta cell density was estimated as an average number of beta cells/islet by dividing the total number of beta cells per section by the total number of islets. The number of beta cells per islet area was calculated for each islet and then averaged.

Selected sections were also examined by confocal microscopy for co-expression of Insulin and Glucagon, using polyclonal guinea pig anti-insulin and rabbit anti-glucagon antibodies (both from Dako, 1:500), and anti-PCNA mouse antibody (Abcam, 1:5000), followed by 2nd donkey antibodies (Jackson Laboratories, 1:500): Alexa-Fluor-488 (anti-rabbit), Alexa-Fluor-647 (anti guinea pig) and Cy-3 (anti-mouse). Mounting and imaging were as above.

2.8. 3D culture of INGAP-MSCs

MSCs grown in monolayers, were trypsinized, washed in serum-free medium and embedded in Matrigel™ (growth factor reduced, Corning, 400 μL +150 μL cells), or Human Collagen type 1 (VitroCol®, Advanced BioMatrix, 419 μL+ 131 μL cells in RPMI/0.1N NaOH) or polysaccharide-based synthetic hydrogel VitroGel®-MSC (2:1 matrix to cells ratio, The Wells Bioscience), following the manufacturer instructions. Typically, the cultures were done in 24-well plates, with the matrix/cell volume of 500–550 μL, overlayered by 500 μL of medium. For culturing in 48-well or 96-well plates, for MTT assay, the volumes were adjusted to 200 and 90 μL, respectively. Plating densities were 1×10^6, 2×10^6, 5×10^6, and 1×10^7 cells/mL. For measurement of INGAP secretion by Western blot, CM was replaced with Opti-MEM for 48 h and collected, and then fresh complete medium was reapplied.

2.9. MTT assay

Viability (cellular metabolic activity) of MSCs cultured in monolayer or embedded in matrices was measured by MTT assay: following treatment in 96- or 48-well plates, 0.5 mg/mL of 3-(4,5-dimethythiazol-2-yl)-2,5-diphenyl tetrazolium bromide (MTT,

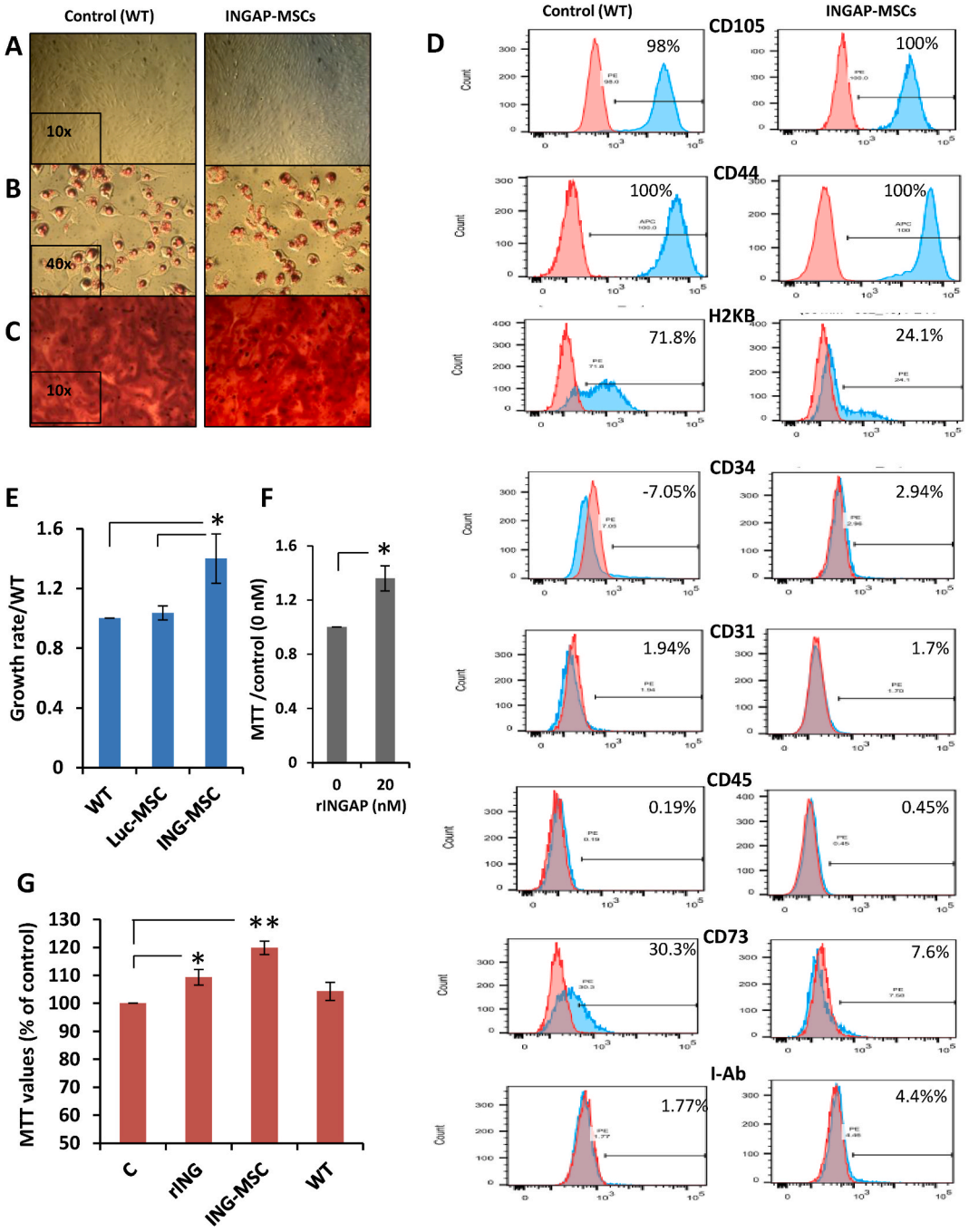

Fig. 2. Characterization of INGAP-MSCs stemness and proliferative potential.

A-C. Differentiation assay: INGAP-MSCs and wild-type (WT) MSCs were exposed to specific differentiation media. **A.** undifferentiated cells; **B.** adipogenic differentiation (Oil Red O); **C.** osteogenic differentiation (Alizarin Red S.) Bright-field images were taken with a Leica DMIL microscope using 10x and 40× objectives, as indicated in the insets. **D.** Flow Cytometry: INGAP - MSCs (blue peaks) are positive for CD105 and CD44 and negative for CD34 and CD45. Isotype controls are in red. Percentage of positive cells in indicated on each histogram. **E.** INGAP-MSCs proliferate at a higher rate than WT and Luc-MSCs. Cells were plated at 3×10^5 per 150 mm plate, trypsinized and counted 3 days later. Shown are total cell numbers normalized to WT values. **F.** rINGAP increases proliferation in WT-MSCs as shown by MTT assay. Cells plated in 48-well plates at 2×10^3 cells/well were exposed to 20 nM rINGAP for 24 h. Shown are MTT values normalized to negative control (PBS). **G.** Conditioned medium (CM) from INGAP MSCs stimulates proliferation in RINm5F cells. INGAP MSCs (AP2-ING) or WT were placed in Opti-MEM for 48 h. CM titrated to contain 1 nM INGAP, or equal volume of WT CM, or 1 nM rINGAP (rING), was added to RINm5F cells grown in 96-well plates for 24 h, followed by MTT assay. MTT reduction values were normalized to control cells (C) receiving equal volumes of Opti-MEM. *$p < 0.05$, **$p < 0.01$ (*t*-test) compared to C.

Sigma-Aldrich) was added for 4 h at 37 °C, 5 % CO_2. Formazan pellets and the matrices were solubilized overnight at 37 °C with 0.01 M HCl+10 % SDS (100 μL/well). Absorbance was measured at 570 nm using microplate spectrophotometer (Bio-Rad). Blanks contained the same volume of medium but no cells.

2.10. RNA extraction and RT-qPCR

MSCs grown in monolayer were lysed in RLT buffer for RNA extraction with RNEasy® Mini kit following the manufacturer's protocol (Qiagen, Toronto, ON, Canada). 3D cultures of MSCs in VitroGel were lysed in QIAzol® (Qiagen) and shredded through a syringe with 22 ½ gauge needle to ensure complete dissolution of the matrix. Following chloroform extraction, aqueous phases were mixed 1:1 with 70 % ethanol and purified with RNEasy Mini kit, as above. 1 μg RNA was reverse-transcribed using the Omniscript kit (Qiagen). Quantitative PCR (3 min activation at 95 °C and 40 cycles at 95 °C–15 s, 58 °C - 10 s and 72 °C–30 s) was performed in CFX96™ Real-Time System (Bio-Rad) using custom-made primers (Supplementary Table 2) and iQ™ SYBR® Green master mix (Bio-Rad). Melt curve analyses were performed to ensure specificity. Samples were run with an inter-plate calibrator and were combined into a gene study by the CFX Manager™ software 3.1 (Bio-Rad) for calculations of the normalized gene expression ($\Delta\Delta C_T$ method) based on three reference genes (GAPDH, SDHA and β-actin), stability of which was confirmed by mean coefficient of variance (CV) being <0.25 and M values < 0.5.

2.11. Statistical analysis

In vitro experiments were repeated at least three times with triplicate samples. Animal experiments were performed twice, with 3–5 animals per group. Results are expressed as means ± SEM. Data were analyzed by one-way ANOVA followed by post hoc tests as appropriate, or by Student's t-test. All analyses were performed using Microsoft Excel and SigmaPlot (v. 15, AlfaSoft). A P value ≤ 0.05 was considered statistically significant for all comparisons.

3. Results

1. Generation of INGAP-expressing MSCs

Intended for animal experiments, INGAP-expressing MSCs were engineered to express Luciferase (Luc) for cell tracking in live animals and GFP for cell sorting. As described in Materials and Methods and illustrated in Supplementary Figs. 1 and 2, the FLAG/DDK tag was added to INGAP cDNA and subcloned into pCMV6 plasmid followed by generating a tricistronic construct in a retroviral vector AP2 [27] (Supplementary Fig. 3) (Luc)–T2A-INGAP–IRES-GFP named AP2-INGAP by PCR cloning (the schematic is shown in Fig. 1A). Transduction of mouse bone marrow-derived MSCs with the resulting retroviral particles achieved simultaneous expression of all three proteins in the cells termed INGAP-MSCs (Fig. 1B). Cells were sorted by FACS (GFP +) to obtain pure populations of INGAP-MSCs for further experiments. Likewise, MSCs transduced with empty vector AP2-Luc retroviral particles were generated and confirmed to express both Luc and GFP but not INGAP (Supplementary Fig. 4).

2. Characterization of INGAP-MSCs

As shown by flow cytometry, INGAP-MSCs have maintained the phenotypic profile characteristic of MSCs, being positive for CD44, CD105, and negative for CD31, CD34, CD45, major histocompatibility complex class II (I-AB), similar to wild type (WT) MSCs (Fig. 2 D). Expression of two other common MSC markers, major histocompatibility complex class I (H2KB) and CD73 (Ecto-5′-nucleotidase) appeared to diminish in INGAP-MSCs. However, these phenotypic differences did not affect the ability of INGAP-MSCs to differentiate into adipocytes, osteocytes (Fig. 2A–C, shown for both INGAP-MSCs and WT-MSCs) and chondrocytes (Supplementary Fig. 7) *in vitro* when exposed to specific differentiation-inducing media, thus suggesting that INGAP-MSCs retained their MSC characteristics.

Expression of a senescence marker, CDK inhibitor p21, anti-apoptotic protein Bcl2 and heat shock proteins HSP70 and Grp78 was assessed in comparison to MSCs of earlier passages (p12-13) derived from a different donor. Of note, these cells were growing slower than INGAP-MSCs (Td was 46.8 ± 5.5 h). These results show that INGAP-MSCs exhibited no sign of senescence or cellular stress judged by the absence of increase in p21or Grp 78, or by the decrease in Bcl-2 relative to the cells of earlier passages (Supplementary Fig. 8), no vacuolization or enlarged morphology. To the contrary, p21 was lower than in p12-13 MSCs, which is consistent with the faster growth and the absence of other signs of senescence such as vacuolization and enlarged morphology. There was no differ ence in Bcl2 expression, while Grp78, involved in the unfolded protein response was downregulated suggesting no ER stress in INGAP-MSCs (Supplementary Fig. 8). Interestingly, the expression of HSP70 was increased about 3-fold relative to earlier passages. Although HSP70 is usually associated with cellular stress, it has also been linked to proliferation [32], which might explain its higher expression in the faster growing INGAP-MSCs.

INGAP-MSCs displayed a slightly higher growth rate than WT or AP2-Luc MSCs (Fig. 2E), with Td of 25.8 ± 1.2 h, versus 30.8 ± 2.9 h (WT) and 30.3 ± 2.3 h (Luc). To test whether INGAP, previously shown to increase proliferation of RINm5F cells, had an autocrine mitogenic effect on INGAP-MSCs, we exposed WT-MSCs to rINGAP for 24 h in dose response experiments. As shown by MTT assay, effective rINGAP concentrations were in the range of 10–40 nM (Fig. 2F, shown for 20 nM, and Supplementary Fig. 9), which is in agreement with the aforementioned rate of INGAP secretion by INGAP-MSCs. The mitogenic activity of the MSC-secreted INGAP was confirmed by treating RIN-m5F cells with INGAP-MSC CM titrated to contain 1 nM INGAP (Fig. 2 G), the concentration proven

effective in previous experiments [23]. Together, these data strongly suggest that the higher growth rate of INGAP-MSCs is driven by autocrine INGAP signaling.

INGAP secretion rates were estimated as ~1 μg/10^6 cells in 48 h, as determined by Western blot densitometry (example shown in Supplementary Fig. 5). This value can be extrapolated to estimate INGAP delivery by INGAP-MSCs when implanted *in vivo*.

3. Implantation of INGAP-MSCs in non-diabetic and diabetic C57BL/6 mice

To determine if INGAP-MSCs were well tolerated by mice and could be tracked by BLI, INGAP-MSCs resuspended in RPMI medium were implanted IP into 8-week-old C57BL/6 mice, normal or rendered diabetic by Streptozotocin (STZ) injection (125 mg/kg), with glycemia of 15.8 ± 0.91 mmol/L on day 7. Weight measurements and glycemia were taken weekly. BLI was performed right after implantation and then weekly for 6 weeks.

Both in non-diabetic and diabetic mice, the Luciferase signals were evenly distributed in the peritoneal cavity immediately after implantation (radiance values taken for 100 %) Fig. 3A–a, d). This was followed by a rapid decline of the signal, in particular in non-diabetic mice, which dropped by 97 % in the first week and displayed a minimal bioluminescence after 2 weeks and by week 6 it became undetectable (red line, Fig. 3 B). In diabetic mice, however, bioluminescence declined less rapidly (to 26 % at week 1, blue line, **B**) as some cells migrated towards the pancreas and remained in the pancreatic region for at least 4–5 weeks, with gradual decline of the signal (Fig. 3 A (d-e), B).

In non-diabetic mice, no changes in weight or glycemia were observed following implantation (Supplementary Fig. 10A and B), indicating a good tolerability of INGAP-MSCs. In diabetic mice, implantation 7 days post STZ was likewise well tolerated with no

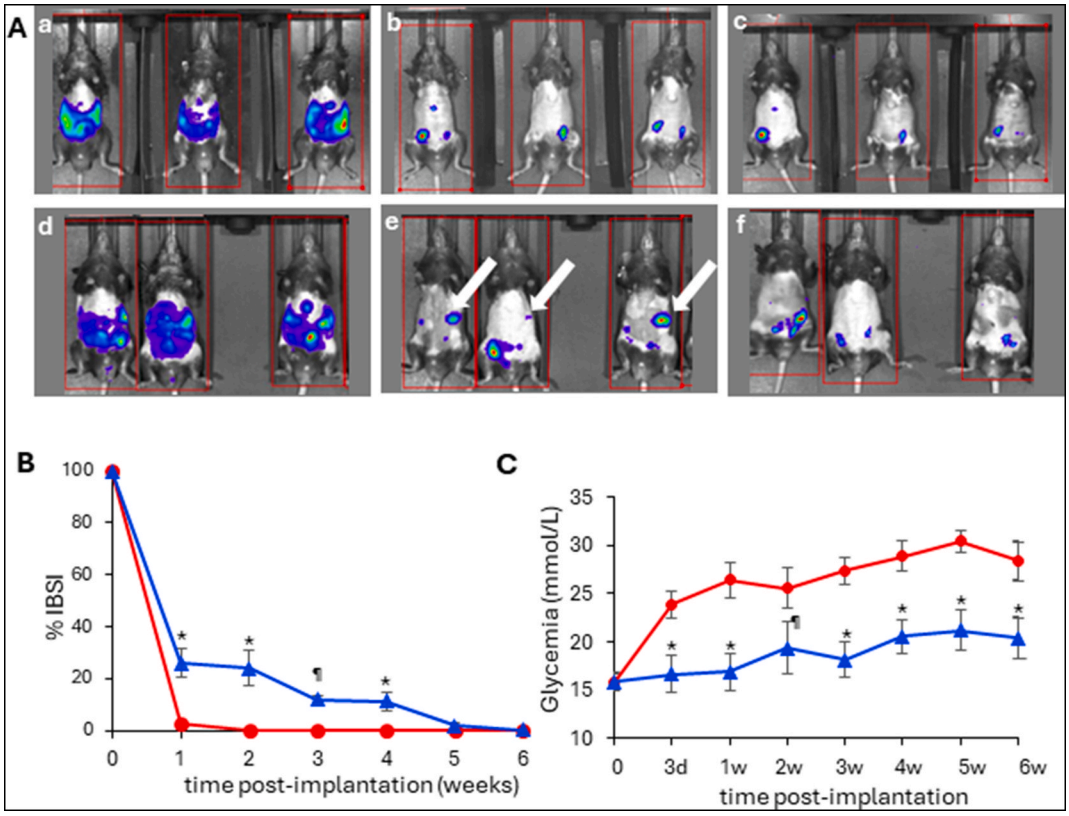

Fig. 3. Implantation of INGAP-MSCs into normal and diabetic C57BL/6 mice: Cell retention and the effect on blood glycemia.
8-weeks old male C57Bl/6 mice normal or rendered diabetic by STZ injection were injected with INGAP-MSCs IP. Bioluminescence was measured immediately and then weekly for 6 weeks.

A. Representative images of the bioluminescent signal at the beginning of the study (**a, d**), after 4 weeks (**b, e**) and after 6 weeks of treatment (**c, f**). Upper panel - normal mice, lower panel - diabetic mice. White arrows indicate accumulation of INGAP-MSCs in the pancreatic region.

B. Dynamics of the cell retention over time was estimated by the IVIS Spectrum CT measurement of bioluminescence and is shown as the percentage of the initial Bioluminescence signal intensity (% IBSI) in the untreated mice (●) or treated with INGAP-MSCs (10^7 cells/mouse) (▲). ¶p < 0.01, *p < 0.05, ANOVA followed by *t*-test.

C. INGAP-MSCs implantation stabilized blood glycemia in diabetic mice. Shown are glycemia values over 6 weeks in STZ-induced diabetic mice untreated (●) or treated with INGAP-MSCs (10^7 cells/mouse) (▲). Data are shown as the Means ± S.E.M. d-days; w-weeks.
*p < 0.01, ¶p < 0.05 by ANOVA followed by pair-wise t-tests.

changes in weight (Supplementary Figure 10C), or behavior. Most interestingly, INGAP-MSCs stopped the climb in glycemia, which continued in the control STZ mice for at least another 7 days (Fig. 3C). This effect was first detected on day 3 and maintained for 6 weeks, at which point the animals were sacrificed and the pancreata examined for insulin expression (DAB with Hematoxylin counterstaining). As shown in representative images in Supplementary Fig. 11, pancreatic sections of both INGAP-MSC mice and STZ control contained islets of various sizes, as well as single beta cells and small clusters (<5 cells). We determined that the number of beta cells per islet was significantly higher in INGAP-MSCs than in STZ control (Fig. 4 A). A closer examination of islet morphology revealed that control islets contained relatively more non-beta cells (Supplementary Fig. 11, **insets a vs. b**), consistent with more extensive immunopositivity for glucagon (Fig. 4C and D) and with a lower proportion of beta cells when measured per islet area (Fig. 4 B). Both groups of mice contained PCNA + cells in the acinar tissue and beta cells pointing at the preservation of proliferative capacity in the diabetic condition (Fig. 4E and F). Small ducts with insulin-positive cells suggestive of ongoing islet neogenesis were observed in both groups of mice, however appeared more frequent in the INGAP-MSCs mice versus control (Supplementary Fig. 11, unlabeled insets, compare A and B). Together, these data suggest that INGAP-MSCs may have a protective effect on pancreatic beta cells against STZ and may also stimulate beta cell proliferation and neogenesis, to be determined in future studies.

Given that INGAP-MSCs rapidly declined in numbers, we reasoned that a stronger anti-diabetic effect of INGAP-MSCs could be achieved by increasing cell retention. Therefore, entrapping INGAP-MSCs in an implantable material allowing for potentially higher cell survival *in vivo* and secretion of therapeutic proteins, as shown in our previous studies [28,33–35], was worth exploring. 5×10^6 INGAP-MSCs (in 150 μl RPMI) were mixed with 400 μL of Matrigel and injected subcutaneously on the back of C57BL/6 mice. The bioluminescent signal localized in the implant (100 % at day 0) decreased in intensity post-implantation but to a lesser degree than after IP cell injection (to 13.1 % at week 1, Fig. 5A–C, compare 5C and 3C)), and stabilizing at roughly 2–3% from 5 to 16 weeks. At this time, mice were sacrificed and examined; the signal was still localized at the implantation site and still detectable (Fig. 5 B). This experiment showed that INGAP-MSCs embedding in Matrigel allows for a longer survival of the cells and the expression of INGAP for up to 16 weeks *in vivo*. No adverse effects or changes in body weight or glycemia were observed in these mice (Supplementary Fig. 10A and B). These encouraging new results prompted us to investigate in more detail how matrix embedding affected INGAP-MSC survival and INGAP secretion.

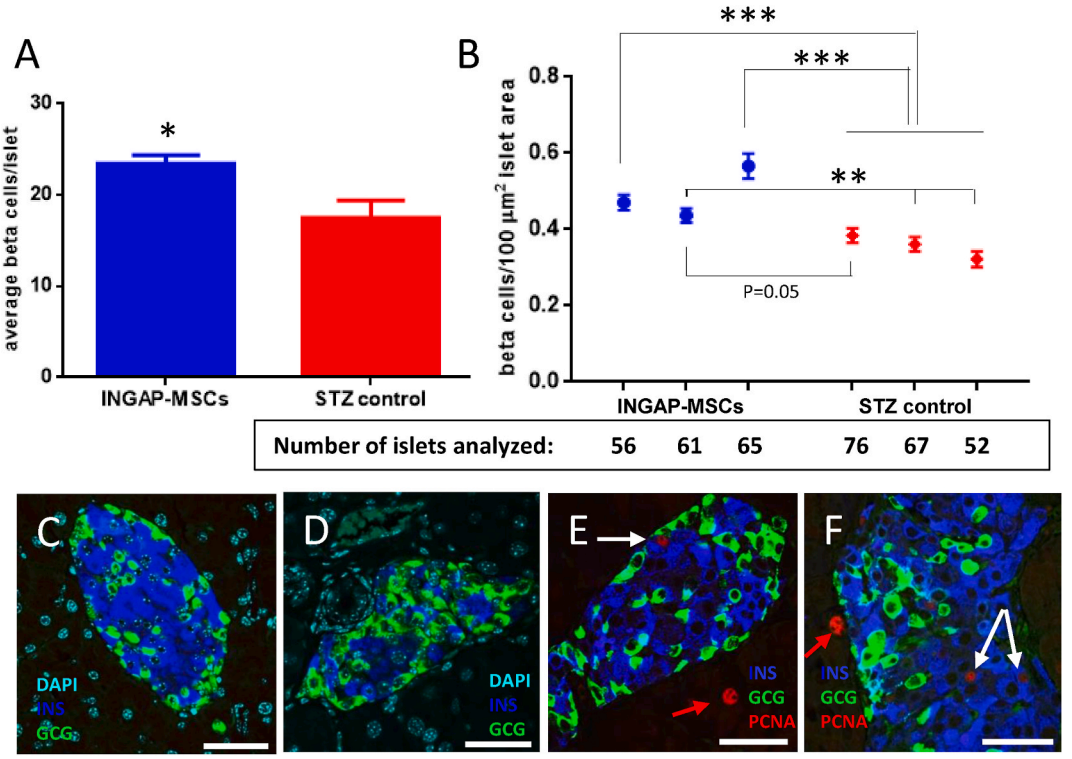

Fig. 4. Islets in INGAP-MSCs treated mice contain more beta cells than STZ control. Islets from 3 pancreatic sections were counted and used to measure the area and to count beta cells (DAB stained) using Fiji/ImageJ. Total numbers of islets per each mouse (n = 3 per group) are shown in the box under the graphs. **A**. Shown is the average number of beta cells per islet per group. **B**. Number of beta cells per islet area is shown for each mouse. Data represent the Mean ± S.E.M. * - $p < 0.05$, ** - $p < 0.01$, *** - $p < 0.001$ (One-way ANOVA with post-hoc Bonferroni test).
C, D. Representative confocal images of islets from INGAP-MSCs (**C**) and STZ-control (**D**) mice immunostained for Insulin (INS) and Glucagon (GCG) show a greater GCG staining in control mice. Nuclei were counterstained with DAPI. **E, F** Sections were additionally probed for PCNA to assess proliferative capacity of pancreatic cells in diabetic animals. Shown are PCNA positive nuclei in the acinar cells (red arrows) and in beta cells (white arrows). DAPI was omitted for clarity of PCNA localization. Bars are 50 mm.

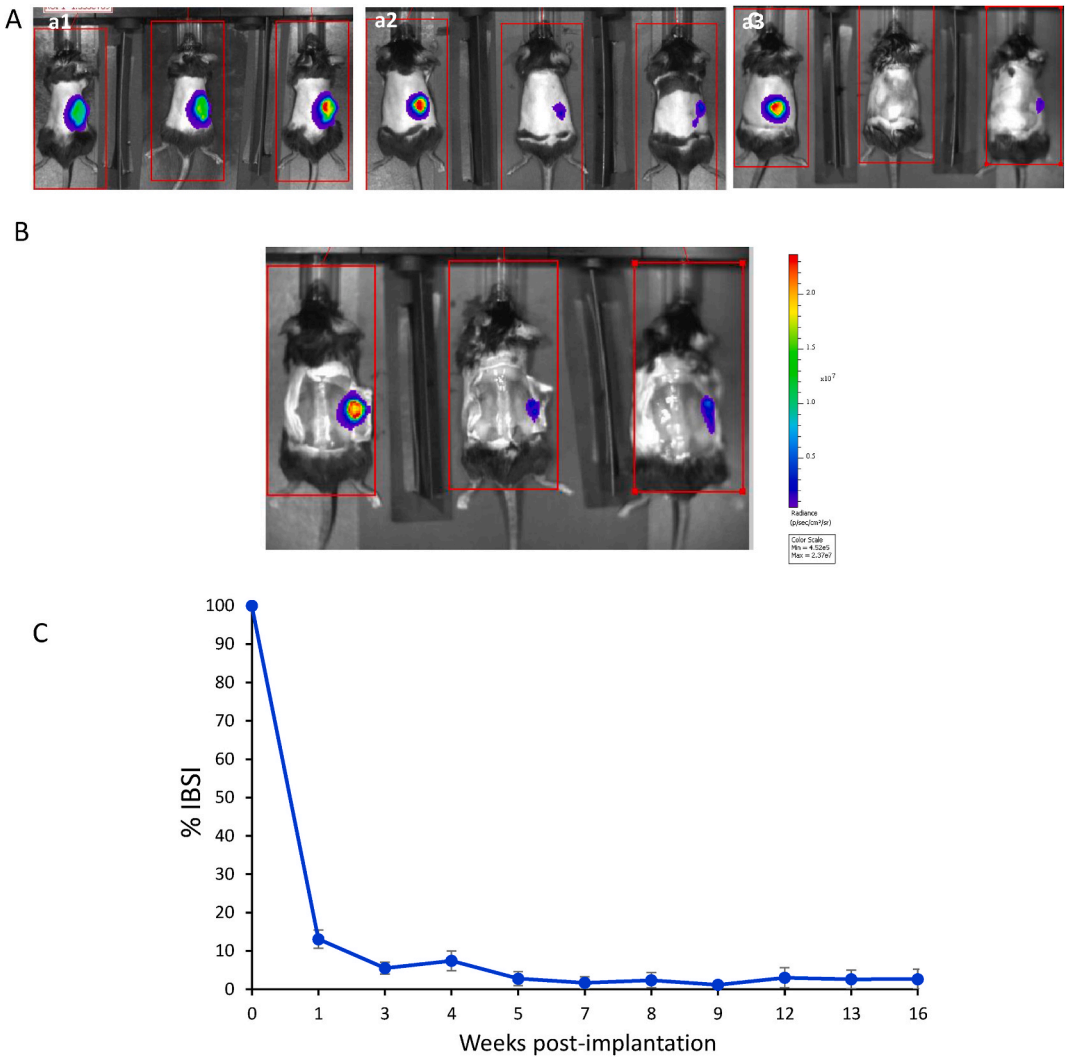

Fig. 5. Dynamics of the retention of Matrigel™– embedded INGAP-MSCs upon implantation into C57BL/6 mice.
8-weeks old male C57Bl/6 mice Normal (n = 4) were injected with INGAP-MSCs embedded in Matrigel ™ and the bioluminescence was measured immediately and then weekly for 15 weeks. **A.** Representative images of the signal at the beginning of the study (**a1**), after 8 weeks (**a2**) and at the end of the 16 weeks (**a3**) duration of the experiment **B.** Persistence of the bioluminescence after 16 weeks. Upon euthanasia, mice from **a3** were imaged with the skin open. **C.** Quantification of the bioluminescence over time measured by the IVIS Spectrum CT, shown as the percentage of the Initial Bioluminescence Signal Intensity (% IBSI).

4. Effects of matrix-embedding on cell survival and INGAP secretion

We chose three commonly used hydrogel matrices, such as ECM-based Matrigel™ and Collagen type 1, and polysaccharide-based VitroGel® MSC. INGAP-MSCs embedded at 1×10^6, 2×10^6, 5×10^6 and 1×10^7 cells/mL were cultured for up to 6 weeks, with quantification of INGAP concentrations in CM weekly by Western blot, as described in Materials and Methods. At 72 h post-embedding (week 0–24 h in regular medium, 48 h in Opti-MEM), we observed density-dependent differences in INGAP concentration between 1×10^6, 2×10^6 and 5×10^6 cells/mL cultures. The values were higher in VitroGel (27.8 ± 4.8 nM– the highest) and Matrigel (25.4 ± 1.48 nM) than in Collagen (20.2 ± 4.4 nM) (Fig. 6**,** week 0). The highest density cultures, 1×10^7 cells/mL (blue line), however, did not show proportionally higher secretion than 5×10^6 cells/mL, suggesting that the density was too high for proper cell function.

One week later, INGAP concentrations increased in VitroGel (all densities) and Matrigel cultures (lower densities) but the effect of density on INGAP secretion became less apparent (Fig. 6). This trend continued over the course of 6 weeks, suggesting that the initial difference in cell numbers diminished as well. Based on these data, plating cells at $1 \times 10^6 - 2 \times 10^6$ cells/mL in Matrigel and VitroGel is optimal long-term, as a higher plating density did not provide further advantage in INGAP secretion. However, for a shorter-term effect, $\leq$3 weeks, 5×10^6 cells/mL may be advantageous. The overall trend in INGAP secretion looked better in VitroGel than in Matrigel, where it gradually declined over time (Fig. 6). The collagen cultures did not demonstrate an increase in INGAP secretion after

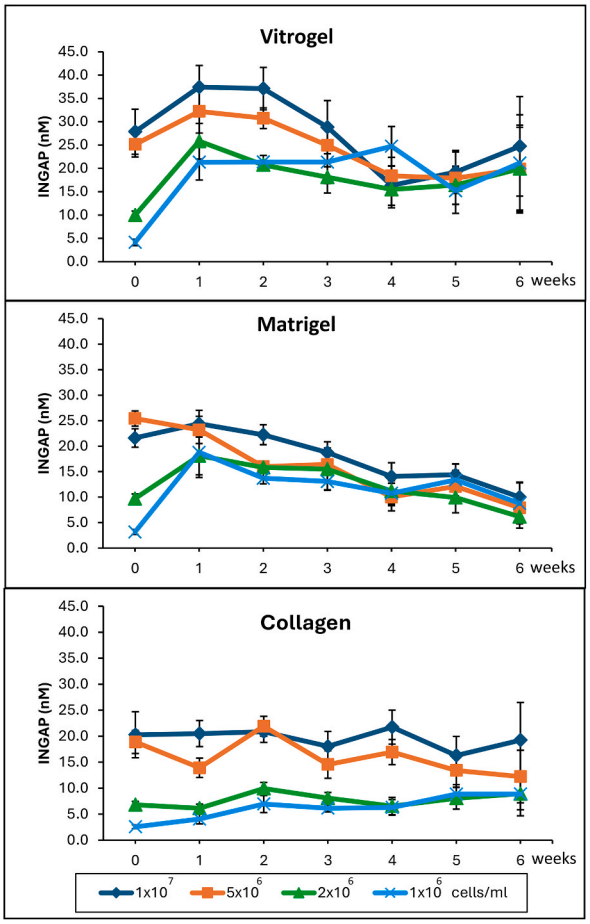

Fig. 6. Image replacement requested - replacement file submitted **INGAP secretion in 3D cultures of INGAP-MSCs gradually declines over time.** INGAP-MSCs were embedded into Vitrogel®-MSC, Matrigel™ or Collagen Type I (VitroCol®) at the densities indicated in the legend and cultivated for 6 weeks. INGAP concentration in CM of 3D cultures was estimated weekly by Western blot analysis, as described in Material and Methods and is shown in Supplementary Fig. 5. Shown are the Means ± SEM; n = 7 for weeks 1–3; n = 6 for weeks 4–5; n = 4 for 6 weeks.

week 1 remaining flat over time and the difference between plating densities was observed for longer. However, the overall secretion level in Collagen was lower than in VitroGel.

It should be noted that the highest INGAP concentrations in CM of VitroGel cultures were lower per cell (based on the plating density) than in the monolayer cultures. Thus, 30 nM INGAP was produced by 0.5×10^6 cells/mL in monolayer in 48 h, while about 10 times more cells in VitroGel (5×10^6 cells/mL) were required to achieve this concentration. In Matrigel and Collagen, the difference was even greater. Whereas it is possible that INGAP was sequestered by the matrix and only a fraction of it was released in the medium, another possibility is that cell survival and functionality was affected by embedding. We evaluated cell viability by MTT assay in 3-week-old matrix cultures done in comparison with freshly embedded cells. The results show a drop in viability after 3 weeks in all three matrices (e.g., to 14.1 % in Matrigel, at 1×10^7 cells/mL) except for cells seeded at$1x10^6$ cells/mL (Supplementary Fig. 12**)**. In line with the INGAP secretion data, best viability was observed in VitroGel, at$1x10^6$ cells/mL, whereas 2×10^6 cells/mL displayed a 70 % survival rate. These data suggest that cell viability is the main factor affecting INGAP secretion rate in matrix-embedded cultures.

5. Spontaneous adipose differentiation of MSCs in the matrices

Upon matrix-embedding, INGAP-MSCs lost their spindle-like morphology and acquired a rounded shape. Within a few days of culture, formation of small lipid droplets was observed and was corroborated by Oil-Red-O staining at day 7 **(**Fig. 7 B, shown for VitroGel). Of note, cells were cultured in the regular growth medium, not in the adipogenic differentiating medium. Similar changes were observed at all plating densities in INGAP-MSCs, in WT MSCs (Fig. 7A) and in Luc-MSCs (data not shown). The adipocyte appearance was maintained for 6 weeks in all three matrices (Fig. 7C–F- shown for VitroGel and Supplementary Figure 13). Analysis of the gene expression in 7-day cultures showed a strong upregulation of adipocyte-related genes, such as the key transcription factor PPARγ, Adiponectin (AdipoQ), Fabp4 and Perilipin 1 (Plin1) (Supplementary Figure 14). Expression of the genes associated with cellular stress, senescence and apoptosis in INGAP-MSCs did not change significantly, as compared with the cells grown in monolayers,

except for HSP70, which was downregulated (Supplementary Figure 8, grey bars). Although INGAP-MSCs differentiated into adipocytes, they continued to express the transgene as evidenced by GFP fluorescence up to 6 weeks (Fig. 7 D), (Supplementary Figure 13), and by continuous secretion of INGAP (Fig. 6).

Adipogenic differentiation of INGAP-MSCs was also observed in the Matrigel implants collected from the mice 15 weeks after implantation. Fig. 7 G and Supplementary Fig. 15 show large numbers of adipocytes of a typical morphology, with the cytoplasm surrounding a large lipid droplet and immunopositive for INGAP (Fig. 7H). Co-expression of perilipin 1 and Luciferase or DDK-tag, both markers of INGAP-MSCs (Supplementary Fig. 16), further confirms differentiation of INGAP-MSCs into adipocytes. Together, these data show that matrix-embedding promotes spontaneous adipogenic differentiation of INGAP-MSCs both *in vitro* and *in vivo* and that this differentiation does not hinder the strong expression of INGAP.

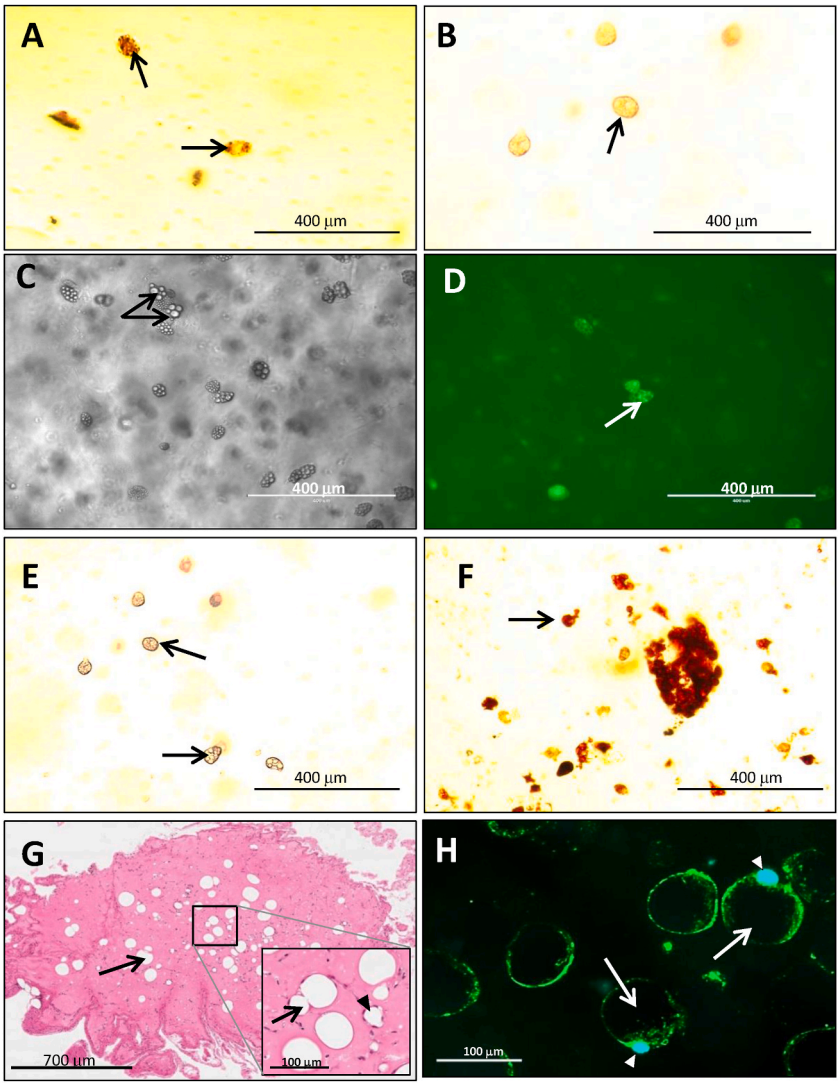

Fig. 7. Adipose differentiation of MSCs embedded in VitroGel® and Matrigel™.
A, B – Oil-Red-O staining of 7-day cultures of WT-MSCs (**A**) and INGAP-MSCs (**B**); images taken with Leica DMIL microscope. **C–F.** INGAP-MSCs embedded for 6-weeks. Shown are: phase contrast (**C**) and GFP (**D**) live images (Invitrogen EVOS-FL microscope); bright field images of live cells (**E**) and formalin-fixed cells stained with Oil-Red-O (**F**, Leica DMIL microscope). **G-H.** Representative images of Matrigel-embedded 5×10^6 INGAP-MSCs 15 weeks post-implantation in C57BL/6 mice: Hematoxylin-Eosin stained section of the implant (**G,** images taken with Aperio AT Turbo Scanner (Leica Biosystems**);** Immunostaining with anti-INGAP/anti-rabbit Alexa Fluor 488 (green) antibodies **(H,** FV10i confocal microscope (Olympus)**)**. Arrows point at lipid -filled cells; black arrowhead indicates a blood vessel (**G**), white arrowheads indicate nuclei of adipocytes stained with DAPI (**H**).

4. Discussion

In this study, we investigated the possibility of MSCs-based delivery of INGAP, capitalizing on our previous successful experience with this cell/gene therapy approach for delivery of soluble gene products [28,34,35], in this case aiming at creating a both anti-inflammatory and regenerative treatment for diabetes.

We generated INGAP-MSCs that co-expressed INGAP, Luciferase and GFP, retained their differentiation capacity and could be expanded in sufficient quantities for implantation, without exhibiting senescence or apoptosis. This was consistent with our previous studies on gene modification of MSCs, e.g., with Epo [28,30,35] and IL-12 [34] and with the general notion that MSCs can be gene-modified while retaining their properties [15]. We observed that although INGAP-MSCs displayed the same level of expression for most phenotypic markers as WT MSCs, expression of major histocompatibility complex class I (H2KB) and CD73 (Ecto-5′-nucleotidase) diminished. The significance of these changes is unclear, as the precise function of these proteins in MSC physiology has not been delineated. Some heterogeneity in MSC markers is common [36], with CD73 reported as the most heterogeneous [37] and potentially related to the anti-inflammatory activity of MSCs [38]. Despite these phenotypic differences, we conclude that INGAP-MSCs retained their MSC properties, primarily the differentiation capacity, and are suitable for the outlined experiments. INGAP secretion was estimated as 1 μg/10^6 cells/48 h. In previous pilot studies (unpublished) we showed that rINGAP, injected IP at 5 μg daily, was effective in reducing hyperglycemia in severely diabetic mice. To achieve this concentration, 1 × 10^7 cells of INGAP-MSCs per mouse were required for implantation.

Since IV injections of MSCs in mice are limited to ~1 × 10^6 cells due to the risk of lung embolism [39], we chose the IP route for implantation, proven successful in our previous studies with Epo-expressing MSCs to achieve the therapeutic effect in the model of acute kidney injury [30].

The results of the implantation experiments can be summarized as follows.

1. INGAP-MSCs are well tolerated by mice and can be tracked by live BLI for a few weeks. The longevity of the BLI signal depended on the route of implantation (IP vs hydrogel patch) and the presence of diabetes – in non-diabetic mice injected IP, the cell retention was the lowest, whereas in diabetic mice the bioluminescence lasted for at least 4 weeks due to the cells migrating towards the pancreas and being able to engraft and persist in that region. This observation is consistent with the known phenomenon of MSC homing to the site of injury [40], however the exact mechanisms of this are poorly understood. It will be interesting to investigate where INGAP-MSCs engraft and whether they are able to reach the islets or localize elsewhere. However, even in diabetic mice the decline in INGAP-MSCs presence was significant during the first week post implantation, consistent with other reports of poor cell survival and retention [41,42]. A strong peritoneal reaction and phagocytosis of MSCs by macrophages has been implicates as the main mechanism underlying the poor cell survival [43].

2. Importantly, despite the low retention in diabetic mice, INGAP-MSCs prevented the further increase of hyperglycemia observed in non-treated STZ control. Our 6-week treatment did not reverse diabetes but kept the glycemia levels significantly lower than in control. We could not estimate the level of INGAP secretion in the mice but based on the cell survival dynamics, it was likely in the lower range than needed for a more robust effect. One can speculate that this effect could have been more significant if cell survival and retention were improved. It is also possible that longer treatment or repeated administrations of INGAP-MSCs would result in a better outcome.

In respect to the potential mechanisms underlying the INGAP-MSCs effects, the comparative histological analyses of the pancreatic sections of these mice demonstrated a higher density of beta cells in islets in the INGAP-MSCs treated mice. This would be in line with the previously described protective properties of INGAP, including its effects on the survival of isolated islets [44,45], anti-cytokine protection in beta cells [29], and prevention of STZ-induced diabetes in INGAP transgenic mice [46]. INGAP has also been shown to stimulate beta cell proliferation and insulin secretion [23,47], which might have also contributed to its anti-diabetic effect observed in this study. Even though we did not observe more PCNA + cells after 6 weeks of treatment, an increase in proliferation early after implantation cannot be excluded. Lastly, a possibility of islet neogenesis from the ductal epithelium, previously described for INGAP [17,21] would be of interest to later explore.

Although the observed effects are most likely mediated by INGAP, some of them could be attributed to MSCs, which have been shown to ameliorate diabetes in animals and humans [6,8,9,11]. Since our study was limited to investigating the survival of INGAP-MSCs in diabetic animals and testing their therapeutic effect in principle, a more detailed investigation into the roles of both INGAP and MSCs is required in the future.

3. Implantation of INGAP-MSCs in Matrigel explored the idea that a hydrogel matrix can provide a supportive microenvironment and, at the same time, allow for the secreted factors to circulate [41]. We show that contrary to the cells implanted in suspension, Matrigel-embedding provided a long-lasting presence of INGAP-MSCs in non-diabetic mice (up to 16 weeks), while maintaining a strong expression of INGAP. These promising data led us to investigate cell survival and INGAP secretion in three hydrogel matrices such as Matrigel® and Collagen type 1, and a synthetic polysaccharide-based hydrogel VitroGel® MSC, specifically designed for MSC expansion *in vitro* and *in vivo*.

The 3D culture data show that cell survival and INGAP secretion in the matrices strongly depended on the cell plating densities, with 1–2 x 10^6 cells/mL being the best in our experiments. Out of three matrixes tested, VitroGel may be the most optimal for both cell survival and INGAP secretion based on the data obtained.

Since the survival and secretion rates are lower in the matrix cultures, additional optimization may be required. For example, one possibility is to increase the level of INGAP expression/cell, whereas improving cell survival rates at a higher cell density is another important avenue to explore. It appears that the steepest decline in cell numbers takes place early after embedding, which might be associated with sudden changes in extracellular cues, mechanical factors, growth factors and cell density, all able to affect cell viability.

Several strategies, such as preconditioning with hypoxia, or cytokines, melatonin [48] or inhibition of TLR4 signaling [49] could be explored.

Interestingly, we found that all MSCs, including WT and AP2-Luc spontaneously differentiated into adipocytes in all three matrices in the regular growth medium, thus suggesting that it was the 3D culture configuration rather than a particular matrix or the gene modifications of the MSCs that was responsible for this effect. This unexpected result was in conflict with several reports, demonstrating that encapsulated MSCs retain their phenotype, e.g. in collagen [50], and with recent reviews promoting the advantages of biomaterial scaffolds, including alginate and collagen, for MSC cultures and implants because of the improved survival and continuing secretion of the paracrine MSC factors [41,51,52]. On the other hand, the differentiation of implanted MSCs into adipocytes has been reported [53] and the challenges associated with maintaining MSCs in undifferentiated state have been highlighted in a recent review [54]. The mechanisms involved in triggering MSC differentiation, or in preserving the undifferentiated state, are quite complex and include guidance from biophysical and biochemical properties of their microenvironment. For example, soft matrices and circular shape have been shown to promote adipocyte differentiation in bone marrow-derived, but not in adipose-derived MSCs, which tend to express neurogenic markers instead [55]. Likewise, adipose differentiation of human MSCs derived from embryonic cells was observed in 3D cultures containing collagen type 1 [56]. This shows that the cell geometry, matrix stiffness and adhesion ligands should be taken into account for tissue engineering strategies to direct MSC fate [54,57]. Among other factors, a higher cell density [58], as well as late cell passages were linked to spontaneous adipose differentiation in mouse MSCs [59]. All these factors could be potentially responsible for the adipose differentiation observed in our study and should be further investigated. We showed that adipo-INGAP-MSCs continued to express INGAP and thus could be used for gene delivery, but the possible loss of mesenchymal stemness might potentially limit their utility as the source of anti-inflammatory and other beneficial molecules inherent to undifferentiated MSCs.

At present, there is no clear understanding of how to prevent the unwanted adipogenic differentiation. Recent studies suggest that higher O_2 levels might be beneficial [60] or suggest overexpressing Sirt1 and Vav1to retard adipogenesis [61]. Other possibilities may lie in developing a different approach to 3D cultures, such as generation of 3D spheroids prior to hydrogel embedding, shown to preserve MSC phenotype [62,63], or macroporous alginate scaffolds that promote cell-cell interactions and improve paracrine function of MSCs [64].

5. Conclusions

In summary, this is the first study reporting INGAP gene transfer into mouse MSCs and successful secretion of INGAP protein as a step in developing a cell and gene therapy for diabetes. The generated cells demonstrated a therapeutic effect in the STZ-treated mice, in a proof-of-concept study. This promising result requires further investigation into the mechanisms of this phenomenon and into optimization of the cell culture and implantation conditions to achieve diabetes reversal. Given the reported clinical safety and efficacy of MSCs for T1DM and T2DM treatment, extending our studies to human MSCs would be of interest.

Ethics statement

All animal work was performed at the LDI Animal Care Facility, in accordance with the Guidelines of the Canadian Council on Animal Care. Animal protocols were approved by the Animal Care Committee of McGill University.

Data availability statement

Data will be made available on request.

CRediT authorship contribution statement

Maria Petropavlovskaia: Writing – review & editing, Writing – original draft, Visualization, Validation, Project administration, Methodology, Investigation, Formal analysis, Data curation, Conceptualization. **Beatrice Assouline-Thomas:** Writing – review & editing, Writing – original draft, Visualization, Validation, Project administration, Methodology, Investigation, Formal analysis, Data curation, Conceptualization. **Jessica Cuerquis:** Visualization, Validation, Methodology, Investigation, Formal analysis, Data curation. **Jing Zhao:** Methodology, Investigation. **Shaun Violette-Deslauriers:** Validation, Methodology, Investigation. **Eni Nano:** Methodology, Investigation. **Nicoletta Eliopoulos:** Writing – review & editing, Supervision, Project administration, Funding acquisition, Conceptualization. **Lawrence Rosenberg:** Writing – review & editing, Validation, Supervision, Resources, Project administration, Funding acquisition, Formal analysis, Conceptualization.

Declaration of competing interest

The authors declare that they have no known competing financial interests or personal relationships that could have appeared to influence the work reported in this paper.

Acknowledgements

This study was funded by the Jewish General Hospital Foundation, Canada (Montreal, QC, Canada), by the Liana's Dream

Foundation, Canada, and by the Réseau ThéCell du FRQS. We acknowledge the technical support of Segal Cancer Centre Research Pathology Facility (RPF) of the JGH and thank Dr. Naciba Benlimane and Lilian Canetti for help with histology, as well as Christian Young for help with Flow Cytometry. We are grateful to Veronique Michaud and the Imaging and Phenotyping Core at the Lady Davis Institute for Medical Research. We also thank Dr. Pierre Paradis and Christophe Goncalves for their help with imaging.

Appendix A. Supplementary data

Supplementary data to this article can be found online at https://doi.org/10.1016/j.heliyon.2024.e35372.

References

[1] M.Y. Donath, et al., Inflammatory mediators and islet β-cell failure: a link between type 1 and type 2 diabetes, J. Mol. Med. 81 (8) (2003) 455–470.
[2] P. Wang, et al., Human beta cell regenerative drug therapy for diabetes: past achievements and future challenges, Front. Endocrinol. 12 (2021) 671946.
[3] J.J. Meier, et al., Sustained beta cell apoptosis in patients with long-standing type 1 diabetes: indirect evidence for islet regeneration? Diabetologia 48 (11) (2005) 2221–2228.
[4] M.M. Gabr, et al., Insulin-producing cells from adult human bone marrow mesenchymal stem cells control streptozotocin-induced diabetes in nude mice, Cell Transplant. 22 (1) (2013) 133–145.
[5] J. Zhang, et al., The challenges and promises of allogeneic mesenchymal stem cells for use as a cell-based therapy, Stem Cell Res. Ther. 6 (2015) 234.
[6] J. Katuchova, et al., Mesenchymal stem cells in the treatment of type 1 diabetes mellitus, Endocr. Pathol. 26 (2) (2015) 95–103.
[7] T.Y. Yeung, et al., Human mesenchymal stem cells protect human islets from pro-inflammatory cytokines, PLoS One 7 (5) (2012) e38189.
[8] Y. Li, et al., Efficacy of mesenchymal stem cell transplantation therapy for type 1 and type 2 diabetes mellitus: a meta-analysis, Stem Cell Res. Ther. 12 (1) (2021) 273.
[9] J. Cho, et al., A review of clinical trials: mesenchymal stem cell transplant therapy in type 1 and type 2 diabetes mellitus, Am J Stem Cells 7 (4) (2018) 82–93.
[10] S.Y. Sun, et al., Efficacy and safety of stem cell therapy for T1DM: an updated systematic review and meta-analysis, J. Diabetes Res. 2020 (2020) 5740923.
[11] L.C. Davies, et al., Type 1 diabetes mellitus donor mesenchymal stromal cells exhibit comparable potency to healthy controls in vitro, Stem cells translational medicine 5 (11) (2016) 1485–1495.
[12] J.N.U. Yaochite, et al., Multipotent mesenchymal stromal cells from patients with newly diagnosed type 1 diabetes mellitus exhibit preserved in vitro and in vivo immunomodulatory properties, Stem Cell Res. Ther. 7 (2016) 14, 14.
[13] P.O. Carlsson, et al., Preserved beta-cell function in type 1 diabetes by mesenchymal stromal cells, Diabetes 64 (2) (2015) 587–592.
[14] U.G. Thakkar, et al., Insulin-secreting adipose-derived mesenchymal stromal cells with bone marrow-derived hematopoietic stem cells from autologous and allogenic sources for type 1 diabetes mellitus, Cytotherapy 17 (7) (2015) 940–947.
[15] N. D'Souza, et al., Mesenchymal stem/stromal cells as a delivery platform in cell and gene therapies, BMC Med. 13 (2015) 186.
[16] V. Mundra, H. Wu, R.I. Mahato, Genetically modified human bone marrow derived mesenchymal stem cells for improving the outcome of human islet transplantation, PLoS One 8 (10) (2013).
[17] R. Rafaeloff, et al., Cloning and sequencing of the pancreatic islet neogenesis associated protein (INGAP) gene and its expression in islet neogenesis in hamsters, J. Clin. Invest. 99 (9) (1997) 2100–2109.
[18] A. Parikh, A.F. Stephan, E.S. Tzanakakis, Regenerating proteins and their expression, regulation and signaling, Biomol. Concepts 3 (1) (2012) 57–70.
[19] R.L. Fleming A, The prospects and challenges for islet regeneration as a treatment for diabetes: a review of islet neogenesis associated protein (INGAP), Diabetes Sci Technol 1 (2) (2007) 231–244.
[20] B. Assouline-Thomas, et al., Production and characterization of the recombinant islet neogenesis associated protein (rINGAP), Protein Expr. Purif. 69 (1) (2010) 1–8.
[21] L. Rosenberg, et al., A pentadecapeptide fragment of islet neogenesis-associated protein increases beta-cell mass and reverses diabetes in C57BL/6J mice, Ann. Surg. 240 (5) (2004) 875–884.
[22] V. Madrid, et al., Islet neogenesis-associated protein pentadecapeptide (INGAP-PP): mechanisms involved in its effect upon beta-cell mass and function, Regul. Pept. 157 (1–3) (2009) 25–31.
[23] M. Petropavlovskaia, et al., Mechanisms of action of islet neogenesis-associated protein: comparison of the full-length recombinant protein and a bioactive peptide, Am. J. Physiol. Endocrinol. Metabol. 303 (7) (2012) E917–E927.
[24] B. Assouline-Thomas, et al., Islet Neogenesis Associated Protein (INGAP) induces the differentiation of an adult human pancreatic ductal cell line into insulin-expressing cells through stepwise activation of key transcription factors for embryonic beta cell development, Differentiation; research in biological diversity 90 (4–5) (2015) 77–90.
[25] J. Li, et al., Islet neogenesis-associated protein-related pentadecapeptide enhances the differentiation of islet-like clusters from human pancreatic duct cells, Peptides 30 (12) (2009) 2242–2249.
[26] K.M. Dungan, J.B. Buse, R.E. Ratner, Effects of therapy in type 1 and type 2 diabetes mellitus with a peptide derived from islet neogenesis associated protein (INGAP), Diabetes Metab Res Rev 25 (6) (2009) 558–565.
[27] J. Galipeau, et al., Vesicular stomatitis virus G pseudotyped retrovector mediates effective in Vivo suicide gene delivery in experimental, Brain Cancer. Cancer Research 59 (10) (1999) 2384–2394.
[28] N. Eliopoulos, et al., Erythropoietin delivery by genetically engineered bone marrow stromal cells for correction of anemia in mice with chronic renal failure, J. Am. Soc. Nephrol. : JASN (J. Am. Soc. Nephrol.) 17 (6) (2006) 1576–1584.
[29] E. Nano, M. Petropavlovskaia, L. Rosenberg, Islet neogenesis associated protein (INGAP) protects pancreatic beta cells from IL-1beta and IFNgamma-induced apoptosis, Cell Death Discov 7 (1) (2021) 56.
[30] N. Eliopoulos, et al., Erythropoietin gene-enhanced marrow mesenchymal stromal cells decrease cisplatin-induced kidney injury and improve survival of allogeneic mice, Mol. Ther. : the journal of the American Society of Gene Therapy 19 (11) (2011) 2072–2083.
[31] J. Schindelin, et al., Fiji: an open-source platform for biological-image analysis, Nat. Methods 9 (7) (2012) 676–682.
[32] K. Helmbrecht, E. Zeise, L. Rensing, Chaperones in cell cycle regulation and mitogenic signal transduction: a review, Cell Prolif. 33 (6) (2000) 341–365.
[33] N. Eliopoulos, et al., A neovascularized organoid derived from retrovirally engineered bone marrow stroma leads to prolonged in vivo systemic delivery of erythropoietin in nonmyeloablated, immunocompetent mice, Gene Ther. 10 (6) (2003) 478–489.
[34] N. Eliopoulos, et al., Neo-organoid of marrow mesenchymal stromal cells secreting interleukin-12 for breast cancer therapy, Cancer Res. 68 (12) (2008) 4810–4818.
[35] N. Eliopoulos, et al., Human-compatible collagen matrix for prolonged and reversible systemic delivery of erythropoietin in mice from gene-modified marrow stromal cells, Mol. Ther. : the journal of the American Society of Gene Therapy 10 (4) (2004) 741–748.
[36] M. Rostovskaya, K. Anastassiadis, Differential expression of surface markers in mouse bone marrow mesenchymal stromal cell subpopulations with distinct lineage commitment, PLoS One 7 (12) (2012) e51221.

[37] F. Haasters, et al., Morphological and immunocytochemical characteristics indicate the yield of early progenitors and represent a quality control for human mesenchymal stem cell culturing, J. Anat. 214 (5) (2009) 759–767.
[38] K. Tan, et al., CD73 expression on mesenchymal stem cells dictates the reparative properties via its anti-inflammatory activity, Stem Cells Int 2019 (2019) 8717694.
[39] L. Sensebe, S. Fleury-Cappellesso, Biodistribution of mesenchymal stem/stromal cells in a preclinical setting, Stem Cells Int 2013 (2013) 678063.
[40] J.L. Liesveld, N. Sharma, O.S. Aljitawi, Stem cell homing: from physiology to therapeutics, Stem Cell. 38 (10) (2020) 1241–1253.
[41] X. Zhao, et al., Constructing a cell microenvironment with biomaterial scaffolds for stem cell therapy, Stem Cell Res. Ther. 12 (1) (2021) 583.
[42] S. Lee, et al., Cell adhesion and long-term survival of transplanted mesenchymal stem cells: a prerequisite for cell therapy, Oxid. Med. Cell. Longev. 2015 (2015) 632902.
[43] C.C. Lachaud, et al., Umbilical cord mesenchymal stromal cells transplantation delays the onset of hyperglycemia in the RIP-B7.1 mouse model of experimental autoimmune diabetes through multiple immunosuppressive and anti-inflammatory responses, Front. Cell Dev. Biol. 11 (2023) 1089817.
[44] M. Zha, et al., Effects of islet neogenesis-associated protein pentadecapeptide on cell mass and insulin secretion of pancreatic beta-cells, J. Endocrinol. Invest. 35 (7) (2012) 634–639.
[45] H. Chen, et al., Islet neogenesis-associated protein-related pentadecapeptide improves the function of allograft after islets transplantation, J. Pediatr. Endocrinol. Metab. 27 (11–12) (2014) 1167–1173.
[46] D.A. Taylor-Fishwick, et al., Islet neogenesis associated protein transgenic mice are resistant to hyperglycemia induced by streptozotocin, J. Endocrinol. 190 (3) (2006) 729–737.
[47] M.I. Borelli, et al., INGAP-related pentadecapeptide: its modulatory effect upon insulin secretion, Regul. Pept. 131 (1–3) (2005) 97–102.
[48] J. Zhao, et al., Melatonin pretreatment of human adipose tissue-derived mesenchymal stromal cells enhances their prosurvival and protective effects on human kidney cells, Am. J. Physiol. Ren. Physiol. 308 (12) (2015) F1474–F1483.
[49] L. Zhao, et al., Preconditioning strategies for improving the survival rate and paracrine ability of mesenchymal stem cells in acute kidney injury, J. Cell Mol. Med. 23 (2) (2019) 720–730.
[50] B.P. Chan, et al., Self-assembled collagen-human mesenchymal stem cell microspheres for regenerative medicine, Biomaterials 28 (31) (2007) 4652–4666.
[51] M. Gionet-Gonzales, et al., Sulfated alginate hydrogels prolong the therapeutic potential of MSC spheroids by sequestering the secretome, Adv Healthc Mater 10 (21) (2021) e2101048.
[52] Y. Huang, X. Li, L. Yang, Hydrogel encapsulation: taking the therapy of mesenchymal stem cells and their derived secretome to the Next level, Front. Bioeng. Biotechnol. 10 (2022) 859927.
[53] U. Kunter, et al., Mesenchymal stem cells prevent progressive experimental renal failure but maldifferentiate into glomerular adipocytes, J. Am. Soc. Nephrol. : JASN (J. Am. Soc. Nephrol.) 18 (6) (2007) 1754–1764.
[54] S. Kidoaki, Frustrated differentiation of mesenchymal stem cells, Biophys Rev 11 (3) (2019) 377–382.
[55] J. Lee, et al., Matrix directed adipogenesis and neurogenesis of mesenchymal stem cells derived from adipose tissue and bone marrow, Acta Biomater. 42 (2016) 46–55.
[56] J.P. Jung, et al., Heterogeneous differentiation of human mesenchymal stem cells in 3D extracellular matrix composites, Biores Open Access 5 (1) (2016) 37–48.
[57] J. Lee, et al., Directing stem cell fate on hydrogel substrates by controlling cell geometry, matrix mechanics and adhesion ligand composition, Biomaterials 34 (33) (2013) 8140–8148.
[58] D.S. Kim, et al., Cell culture density affects the stemness gene expression of adipose tissue-derived mesenchymal stem cells, Biomed Rep 6 (3) (2017) 300–306.
[59] S. Gou, et al., Spontaneous differentiation of murine bone marrow-derived mesenchymal stem cells into adipocytes without malignant transformation after long-term culture, Cells Tissues Organs 191 (3) (2010) 185–192.
[60] L.B. Buravkova, et al., Differential expression of bipotent commitment-related genes in multipotent mesenchymal stromal cells at different O(2) levels, Dokl. Biochem. Biophys. 491 (1) (2020) 67–69.
[61] P. Qu, et al., Vav1 regulates mesenchymal stem cell differentiation decision between adipocyte and chondrocyte via Sirt1, Stem Cell. 34 (7) (2016) 1934–1946.
[62] K.C. Murphy, S.Y. Fang, J.K. Leach, Human mesenchymal stem cell spheroids in fibrin hydrogels exhibit improved cell survival and potential for bone healing, Cell Tissue Res. 357 (1) (2014) 91–99.
[63] S.S. Ho, et al., Increased survival and function of mesenchymal stem cell spheroids entrapped in instructive alginate hydrogels, Stem Cells Transl Med 5 (6) (2016) 773–781.
[64] T.H. Qazi, et al., Biomaterials that promote cell-cell interactions enhance the paracrine function of MSCs, Biomaterials 140 (2017) 103–114.